Premelting and formation of ice due to Casimir-Lifshitz interactions: Impact of improved parameterization for materials

Yang Li [1,2,*] Kimball A. Milton [3,†] Iver Brevik [4,‡] Oleksandr I. Malyi [5] Priyadarshini Thiyam [6]
Clas Persson [7,8] Drew F. Parsons,[9] and Mathias Boström [7,§]

[1]*Department of Physics, Nanchang University, Nanchang 330031, China*
[2]*Institute of Space Science and Technology, Nanchang University, Nanchang 330031, China*
[3]*Homer L. Dodge Department of Physics and Astronomy, University of Oklahoma, Norman, Oklahoma 73019, USA*
[4]*Department of Energy and Process Engineering, Norwegian University of Science and Technology, NO-7491 Trondheim, Norway*
[5]*Renewable and Sustainable Energy Institute, University of Colorado 4001 Discovery Drive, Boulder, Colorado 80309-029, USA*
[6]*Stranski-Laboratorium für Physikalische und Theoretische Chemie,
Institut für Chemie, Technische Universität Berlin, 10623 Berlin, Germany*
[7]*Centre for Materials Science and Nanotechnology, Department of Physics,
University of Oslo, P. O. Box 1048 Blindern, NO-0316 Oslo, Norway*
[8]*Department of Materials Science and Engineering, Royal Institute of Technology, SE-100 44 Stockholm, Sweden*
[9]*Department of Chemical and Geological Sciences, University of Cagliari, Cittadella Universitaria, 09042 Monserrato, CA, Italy*

Recently, the premelting and formation of ice due to the Casimir-Lifshitz interaction, proposed in early 1990s by Elbaum and Schick [Phys. Rev. Lett. **66**, 1713 (1991)], have been generalized to diverse practical scenarios, yielding novel physical intuitions and possibilities of application for those phenomena. The properties of materials, in particular, the electrical permittivity and permeability, exert significant influence on the Casimir-Lifshitz energies and forces and hence on the corresponding premelting and formation of ice. To address these influences in detail and explore the resulting physics, here we revisit and extend the analyses of previous work with both the dielectric data utilized there and the latest dielectric functions for ice and cold water. For the four-layer cases considered by some of us, the existence of stable configurations depending on the initial conditions has been confirmed, and different types of stability corresponding to minima of the Casimir-Lifshitz free energy are demonstrated. As the new dielectric functions for ice and cold water deviate considerably from those used by Elbaum and Schick, their vital impact on three- and four-layer configurations is therefore being reconsidered.

I. INTRODUCTION

Relevant surface free energies should be carefully evaluated when considering the formation of ice and water layers. An important contribution to the theories for surface forces came from Casimir [1], who related the force between a pair of neutral planar perfect metal surfaces to changes in the zero-point energy of vacuum. Later, a much more general theory was derived by Lifshitz and co-workers for interactions between surfaces [2,3]. Attempts to verify the Lifshitz formula [2,3] were taken quite early using surface force measurements [4–6], although those were far from conclusive. Much more definitive were studies of thin-film growth [7–9]. It was in parallel extensively studied theoretically, for instance, by the groups led by Parsegian and Ninham [10–14]. Since the late 1990s, accurate measurements for Casimir forces between metal surfaces were carried out by Lamoreaux and co-workers

[15–17] and later by others [18–20]. The zero-temperature theory has been rather well verified, but the finite-temperature correction, especially for systems consisting of imperfect metals, remains controversial [18–25]. The books by Milton [26], Bordag *et al.* [27], Dalvit *et al.* [28], Buhmann [29,30], and Sernelius [25] describe well this active and important research topic.

Notably, interesting phenomena and applications also come from the finite-temperature Casimir-Lifshitz formula. For instance, the potential role of Casimir-Lifshitz free energy in ice premelting [31] and formation [32] was put forward by Elbaum and Schick. In the specific context of ice/water systems, it has in particular been shown that Casimir-Lifshitz forces [31–37], combined with double layer forces due to experimentally unknown impurity charges [33,38,39], can give rise to short-range repulsion and long-range attraction leading to an equilibrium system with the experimentally observable partial ice premelting [40–44]. The existence of thin surface films of liquid water on ice particles [45,46] has been proposed as a factor influencing environmental physics, including potential effects on frost heave [47] and charging of thunderclouds [48–50]. Based on experimental observations, heat insulating gas hydrate strata was proposed to play

*leon@ncu.edu.cn
†kmilton@ou.edu
‡iver.h.brevik@gmail.com
§mathias.bostrom@smn.uio.no

a role for the internal geophysics on Pluto [51] and the moon Enceladus [52]. Both the chemical composition and the insulating properties for large-scale heat insulating strata on, e.g., the moon Enceladus could be influenced by formation of Casimir-Lifshitz energy-induced micronsized ice layers on the interface between gas hydrate clusters and the salty ocean water [53,54].

In an expansion of the work by Elbaum and Schick [31,32], we predicted that ice could form at a water-silica interface at the triple point of water [36]. This is an update and expansion of that paper, and the purpose is quadruple. First, we will compare our past predictions about the ice formation on silica surfaces, which are based on ice and water dielectric functions from Elbaum and Schick [31], with predictions based on different revised and improved dielectric functions for ice [55,56] and water [55–57] at the triple point of water. Second, this also encourages us to take a careful look at the results obtained by Elbaum and Schick for ice premelting [31] and ice formation on water surfaces [32]. The contradictory results found deserve careful inspection, and the significant dependence on the dielectric functions of media should be emphasized. Third, we use a new theory for Casimir-Lifshitz free energies in inhomogeneous media [58] to explore some generalized cases beyond the three-layer system described by the original Lifshitz theory. Finally, we have detected a minor error of ours in Ref. [36]. This brings about a better agreement between results obtained by using *ab initio* calculated dielectric functions for silica materials [59] and those using experimental dielectric functions (the latter derived from a paper by van Zwol and Palasantzas [60] but treated incorrectly in Ref. [36]).

This work is organized as follows: In Sec. II, we present the theory, including the generalized case where more than one layer are allowed to expand at the expense of other layers [55,61], and we also discuss relevant configurations. As has been demonstrated in our past work [36], with the *ab initio* dielectric functions for silica materials [59] and the experimentally based dielectric functions from Elbaum and Schick [31,32] for ice and water, an ice layer could grow between the water and the silica interface. Within the models applied, this previous result is correct as shown in Sec. III. We will demonstrate that when a minor error in Ref. [36] is corrected, plausible results follow, which are consistent with the results [36] obtained using silica dielectric functions from both Malyi *et al.* [59] and Grabbe [62]. We explore and expand both our past work [36] and those of Elbaum and Schick [31,32] in the light of the new improved dielectric functions for ice and water. In Sec. IV, we try to provide some detailed discussions on the results demonstrated in Sec. III. A simple characteristic parameter method is proposed to facilitate the estimation of the stability properties influenced by the Casimir-Lifshitz interaction. Conclusions are given in Sec. V. Details of a method to evaluate the four-layer Casimir-Lifshitz free energy are provided in the Appendix.

II. THEORY

The natural units $\hbar = c = \varepsilon_0 = \mu_0 = k_B = 1$ are used, unless specified in the current publication. In our previous work [36], we considered a planar-layered system consisting

of silica, ice, and water. The Casimir-Lifshitz free energy in such a three-layered planar geometry (Dzyaloshinskii-Lifshitz-Pitaevskii or DLP configuration for short), where media 1 and 3 are separated by medium 2 with a thickness d [for example, Fig. 1(a)], is well known [2,3]

$$F = T \sum_{n=0}^{\infty}{}' \int \frac{d^2 k}{(2\pi)^2} \sum_{s=\mathrm{E,H}} \ln\left(1 + r_{32}^s r_{21}^s e^{-2\kappa_2 d}\right), \quad (1)$$

the prime means the $n = 0$ term is half-weighted. The reflection coefficients for transverse electric (TE, $s = \mathrm{E}$) are defined as

$$r_{ij}^{\mathrm{E}} = \frac{\kappa_i \mu_j - \kappa_j \mu_i}{\kappa_i \mu_j + \kappa_j \mu_i}, \quad \kappa_i = \sqrt{k^2 + \varepsilon_i(i\zeta_n)\mu_i(i\zeta_n)\zeta_n^2}, \quad (2)$$

in which the electromagnetic response properties of medium i are described by the permittivity ε_i and permeability μ_i. Here, $\zeta_n = 2\pi T n$ is the Matsubara frequency at the temperature T. The transverse magnetic (TM, $s = \mathrm{H}$) counterpart of r_{ij}^{E} is obtained by making the substitution $\varepsilon \leftrightarrow \mu$. In this paper, we focus on the nonmagnetic media.

Very recently, Parashar *et al.* [63], Li *et al.* [58], Esteso *et al.* [61], and Luengo-Márquez and MacDowell [55,56] demonstrated how to expand the Lifshitz theory to the case containing two intermediate layers that can both grow or decrease at the expense of each other. For the four-layer system illustrated by Fig. 1(b), the Casimir-Lifshitz free energy between medium 1 and 4 is derived with the method proposed in Ref. [58] as (for an alternative derivation, please refer to the Appendix)

$$F_{14} = T \sum_{n=0}^{\infty}{}' \int \frac{d^2 k}{(2\pi)^2} \sum_{s=\mathrm{E,H}} \ln\left[1 + \frac{(1 + r_{32}^s)r_{43}^s e^{-2\kappa_3 d_3}}{1 + r_{43}^s r_{32}^s e^{-2\kappa_3 d_3}}\right.$$
$$\left. \times \frac{(1 - r_{32}^s)r_{21}^s e^{-2\kappa_2 d_2}}{1 + r_{32}^s r_{21}^s e^{-2\kappa_2 d_2}}\right], \quad (3)$$

where d_2 and d_3 are the thicknesses of media 2 and 3, respectively. When media 2 and 3 are the same, then the reflection coefficients r_{32}^{E} and r_{32}^{H} are both zero, which means Eq. (3) reduces to the DLP free energy as in Eq. (2). When Casimir-Lifshitz free energies of the the slab 1-2-3 and 2-3-4 DLP configurations are included, then the total free energy $F = F_{14} + F_{13} + F_{24}$ is expressed as

$$F = T \sum_{n=0}^{\infty}{}' \int \frac{d^2 k}{(2\pi)^2} \sum_{s=\mathrm{E,H}} \ln\left(1 + r_{43}^s r_{32}^s e^{-2\kappa_3 d_3}\right.$$
$$\left. + r_{32}^s r_{21}^s e^{-2\kappa_2 d_2} + r_{43}^s r_{21}^s e^{-2\kappa_3 d_3 - 2\kappa_2 d_2}\right), \quad (4)$$

which is consistent with the results presented by Esteso *et al.* [61] and more recently by Luengo-Márquez and MacDowell [55]. (Since in the 4-media case there are three reflection coefficients, one might think that terms with three reflection coefficients could appear. Such terms, however, are forbidden by parity invariance; only even powers of reflection coefficients can appear in the free energy.)

According to Eq. (1) and Eq. (2), when conditions, such as $r_{32}, r_{21} > 0$, are properly satisfied so that the Casimir-Lifshitz free energy depends on the separation between medium 1 and 3 as a monotonically decreasing function, then a repulsive
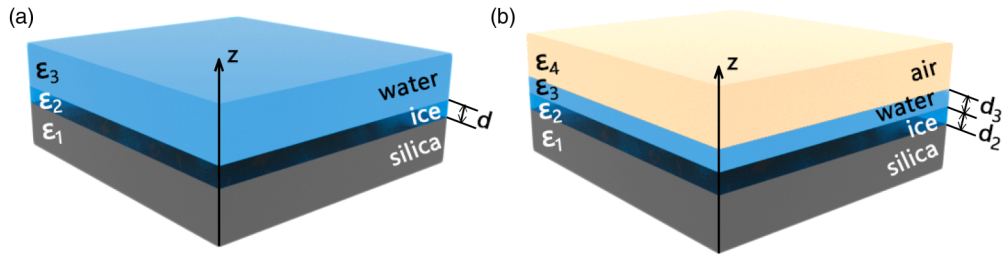
FIG. 1. Schematic illustrations for three- and four-layer configurations. (a) A example of a three-layer configuration, namely, silica-ice-water. (b) A example of four-layer configuration, namely, silica-ice-water-vapor.

Casimir-Lifshitz force is found. This implies that the expansion of the intermediate medium 2 decreases the free energy, forming a more stable system. As has been known since Ref. [3], this kind of condition could typically be satisfied if $\varepsilon_1 > \varepsilon_2 > \varepsilon_3$ or $\varepsilon_1 < \varepsilon_2 < \varepsilon_3$. This repulsion has already been observed in experiments [9,64]. Similarly, if the free energy increases with the separation, an attractive Casimir-Lifshitz force results, which means the system would tend to eliminate the intervening medium to stabilize itself. Therefore the electromagnetic response properties of media will be significant to the stability induced by the fluctuating electromagnetic field. Moreover, when two bulk media interact via more than one intervening medium, multiple stabilities could show up, implying more complicated possibilities and phenomena.

The thermodynamic aspects of the problem can be discussed in simple terms when we require, as here, the temperature to be constant. The thermodynamic potential of interest is then the free energy F, defined as $F = U - TS$, where U is the internal energy and S is the entropy. The Casimir pressure at thermal equilibrium is $p = -(\partial F/\partial d)_T$, where d is the width of the layer. This leads to the following expression for the force density in the inhomogeneous boundary layer, $\mathbf{f} = -\frac{1}{2}\mathbf{E}^2\nabla\varepsilon$. The Casimir force is thus zero in homogeneous regions and there are no longitudinal tensile stresses (no surface tension) in the plane boundary, in contrast to what had been the case if the boundary were curved. The free energy, in turn, is connected with the canonical ensemble in statistical mechanics. Going on to stability issues, one has to consider second-order variations of the free energy. Under a small external disturbance, the mechanical work needed to bring the system from its equilibrium state to a neighboring state is positive. This means at the triple point of water, the coexistence of the three phases with fixed temperature and equal chemical potentials in equilibrium, the Helmholtz free energy should be minimized. In even more complicated cases, such as dielectric fluid exposed to an electric field, the free energy tends toward a minimum. The central inequality becomes $(\partial\mu/\partial\rho)_{\mathbf{D},T} > 0$, where μ is the chemical potential per unit mass, ρ the density of the fluid, and $\mathbf{D}$ the electric displacement. This case is general enough to include electrostriction also. A detailed discussion of this situation can be found in Ref. [65]. In turn, it is built on the presentation in Landau and Lifshitz [66], Sec. 18.

Even though we investigate the Casimir-Lifshitz interaction in this paper, it is noteworthy that in realistic environments, such as the ocean, permafrost, or aerosphere, various surface effects, for instance the salt effect, exert their influences on the premelting and formation phenomena. Most

recently, electron tunneling effects (forming an electric double layer in vacuum) have been proposed to enhance heat transfer [67] and friction [68] between metal surfaces, requiring important modifications to the reflection coefficients. Although we here work with dielectrics, rather than metals, in thermal equilibrium in aqueous environment, the electric double layer due to ions in solution is anticipated to be indispensable in our studies, especially when liquid water is an intermediate layer (our four-layer case). However, the effect of aqueous ions on the dielectric function of water and therefore on reflection coefficients is low except at extremely high salt concentrations (exceeding 1 mol/l)[69]. The impact of electrostatic energies of aqueous ions is likely to be more significant than their indirect impact on the Lifshitz interaction. Nevertheless, the possibility of tuning the premelting and formation of ice externally, controlling the heat flux with an external electric field [70,71], is also worth pursuing for both theoretical and practical benefits.

In the following section, some realistic cases will be investigated to acquire an explicit understanding of the role of Casimir-Lifshitz free energy in the premelting or formation of ice in these cases and its generalizations.

III. RESULTS

A. Results using Elbaum and Schick models for ice and water

In this part, we recheck and extend some previous work. In Ref. [36], we studied ice growth on the interface of silica and water, i.e., the silica-ice-water system, at the triple point of water. The dielectric functions for ice and water are taken from Elbaum and Schick [31,32]. As for dielectric functions of silica with various nanoporosities, previous first-principles evaluation [59], together with the phonon contributions counted, is employed [36]. To make comparisons, we also used silica data from Grabbe [62] and from van Zwol and Palasantzas [60]. The dispersions of dielectric functions of ice, water, and silica materials are plotted in Fig. 2, where the error in the calculation when using the data from van Zwol and Palasantzas [60] in our previous paper [36] has been corrected.

With the corrected data, Casimir-Lifshitz free energies of silica-ice-water systems with various silica materials are demonstrated in Fig. 3. Although the corrections do not qualitatively change our result, that is, a nano-sized ice film could form between water and silica, quantitatively undeniable variations happen, for instance, the magnitude of the minimum free energy for the data set 1 of van Zwol *et al.* is only about one-third of that in previous work [36]. Actually this quanti-
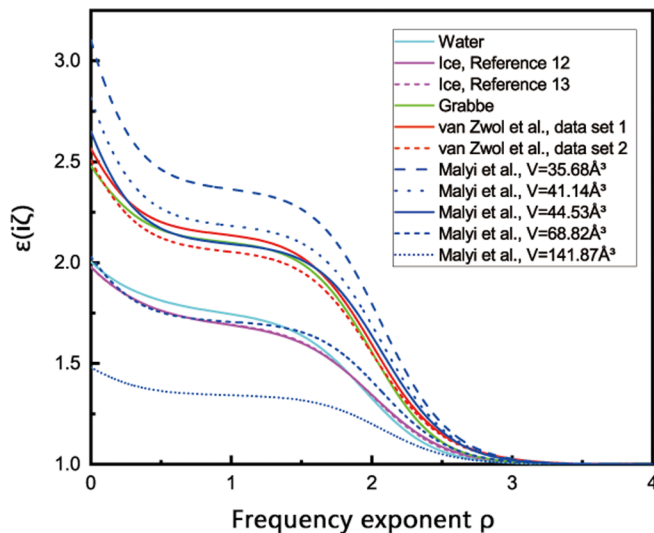
FIG. 2. Permittivities of water (cyan), ice (magenta), and different silica materials (green, red, and blue for Grabbe [62], van Zwol *et al.* [60], and Malyi *et al.* [59], respectively) as functions of frequency exponent ρ. The frequency (in units of rad/s) ζ is related to the exponent $\rho = \log_{10} \zeta / \zeta_T$, in which $\zeta_T = 2\pi T$ is the $n = 1$ Matsubara frequency at the temperature of the triple point of water, 273.16 K. The static dielectric constants for ice and water are, respectively, 91.5 and 88.2 as in Ref. [31], while for SiO$_2$ materials, their static values are 4.97, 4.32, 3.90, 2.62, and 1.69 from Ref. [59] for average volumes per SiO$_2$ V = 35.68, 41.14, 44.53, 68.82, and 141.87 Å^3, respectively, 3.80 for Grabbe [62] and 3.90 for data set 1 and data set 2 of van Zwol *et al.* [60]. The UV contributions of the ice dielectric function are modeled according to Refs. [72,73], which are, respectively, Reference 12 and Reference 13 quoted in Ref. [31].

tative sensitivity with the properties of material (mainly the permittivity in our study here) is not uncommon and deserves considerable care. The ice-water-vapor system investigated by Elbaum and Schick [31,32] is a good example. As shown in Fig. 4, the results by Elbaum and Schick [31] have been rederived with the ice modeled according to Reference 12 cited in Ref. [31] or Ref. [72]. The minimum of the Casimir-Lifshitz free energy is reached when the thickness of the water layer is about 36 Å. However, when the Reference 13 of Ref. [31] or Ref. [73] model of ice in the UV region is employed, the premelting water layer still appears, but with a thickness around 22 Å. Given the fact that the deviation between the two dielectric constant models for ice is less than 1%, the deviations resulting from differences of these two UV models for ice are quite striking. It is thus clear that to achieve an accurate quantitative prediction for the experimental exploration, highly reliable data about the dielectric functions of materials involved are crucial.

Apart from the electromagnetic properties, the structure of the system can also provide remarkable diversities. Esteso *et al.* [61] have investigated the premelting of a thin ice layer absorbed on a quartz rock surface through the stress tensor approach. The consistency with Refs. [31,36] justified their method, and multiple stable states for a given total thickness of ice and water layers were seen. Here we utilize the free energy approach in the hope to clarify relevant properties of the
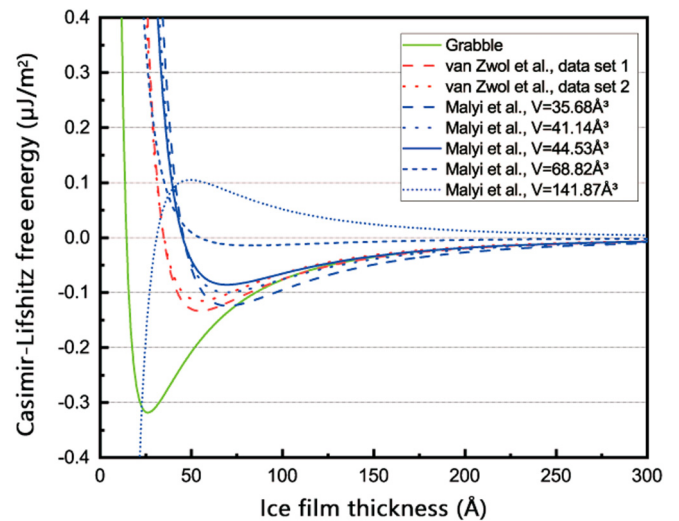

FIG. 3. The Casimir-Lifshitz free energy per unit area for silica-ice-water configuration at the triple point of water as a function of the thickness of ice layer. Its dependence on silica permittivities, thus the nanoporosities, is shown.

silica-ice-water-vapor system. As shown in Fig. 5(a), for the silica material with average cell volume $V = 35.68$ Å^3, in the d_2-d_3 plane (here d_2 and d_3 are the thicknesses of ice and water layers, respectively), there are two regions, i.e., the green and blue trenches, where the Casimir-Lifshitz free energy minimizes itself locally. On other parts of that plane, however, the free energy will finally fall into either trench whenever
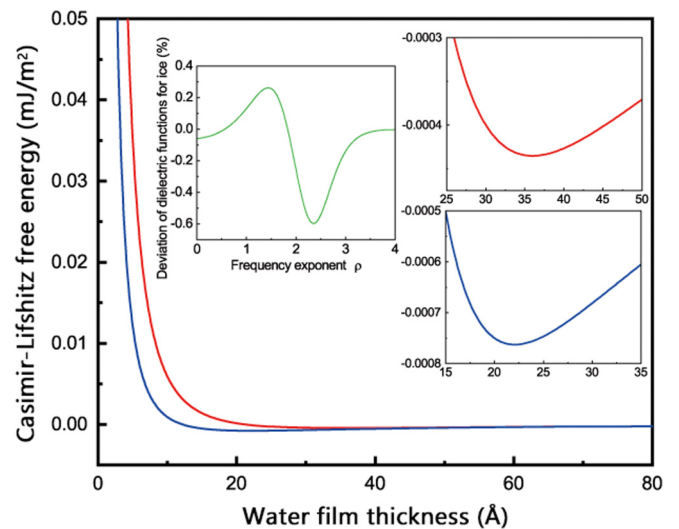

FIG. 4. The Casimir-Lifshitz free energy of ice-water-vapor system as a function of water layer thickness. The results are obtained based on the data used by Elbaum and Schick in Ref. [31]. The Casimir-Lifshitz free energies are plotted with the UV models for the ice dielectric function given by Reference 12 (red) and Reference 13 (blue) cited in Ref. [31], respectively. The behavior near the minima is shown in the right insets. The deviation between the dielectric functions for ice with different UV models, denoted ε_{12} and ε_{13}, is defined as $(\varepsilon_{13} - \varepsilon_{12})/\varepsilon_{12}$. Its dependence on the frequency exponent ρ is given in the middle inset.
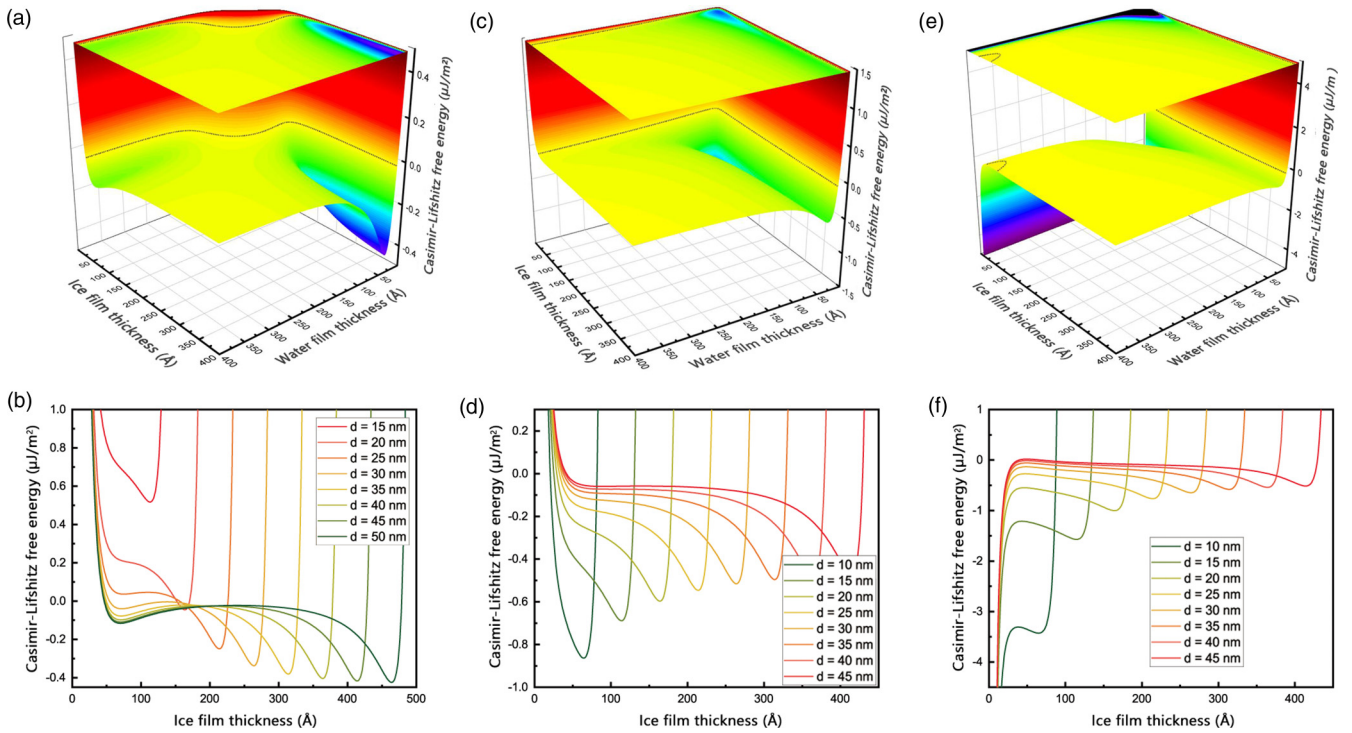
FIG. 5. The Casimir-Lifshitz interaction free energy of silica-ice-water-vapor system at $T = 273.16$ K with the average volume per SiO_2 being $V = 35.68$ Å^3 (a and b), $V = 68.82$ Å^3 (c and d), and $V = 141.87$ Å^3 (e and f). The dielectric functions for ice and water from Elbaum and Schick [31,32] are employed. For subfigures a, c, and e (the corresponding projection of each 3D surface is given at the top), the dependence of free energy on the thicknesses of ice and water films are demonstrated. For subfigures b, d, and f, the dependence of free energy as the function of ice film thickness, with the total thickness of ice and water layers fixed as d, is given.

possible, depending on the initial state. If the amount of water absorbed on this silica material is almost fixed, such that the total thickness of ice and water layers can be regarded as a constant, then the minimum of Casimir-Lifshitz free energy, as demonstrated in Fig. 5(b), would be split into two by increasing total thickness $d = d_2 + d_3$. The depths of the two minima increase much slower than does the distance between them, which may signify a clear separation between the two phases and facilitate possible experimental investigations. If the average cell volume of SiO_2 is increased to $V = 68.82$ Å^3, then only one physically nontrivial minimum trench survives, and there is a global minimum of free energy on the d_2-d_3 plane (at about $d_2 = 3.2$ nm and $d_3 = 3.9$ nm). In addition, by attaching more water to this silica material, the ice layers will keep growing and the water layer always remains in the nanoscale. If the average cell volume is further increased to about $V = 141.87$ Å^3, the property of stability will be radically changed, as illustrated in Fig. 5(e). The strong stability is now at $d_2 = 0$, which means then the system is stabilized when the ice layer vanishes. If an ice layer is put on this silica, its thickness will determine whether it could melt easily. On the other hand, when a water layer is on this silica, the Casimir free energy prevents the formation of ice at the silica-water interface.

B. Results using recent models for ice and water

Recently, Fiedler *et al.* [57] reanalyzed the available data for the optical spectra for water. A careful parametrization

for ice-cold water was performed, which simultaneously fitted both the real and the imaginary parts of the dielectric function at real frequencies. Preliminary calculations using the new dielectric function for water [57] together with the older dielectric function for ice [31] resulted in a prediction that micron-sized ice layers can form at water surfaces. This is in contrast to the work by Elbaum and Schick [31,32], in which the ice premelting [31] due to dispersion forces was predicted, while no ice formation on water surfaces [32] was seen. Considering the importance of this topic, we revisit this problem using the most recently reported dielectric functions for both ice and water obtained by Luengo-Márquez and MacDowell [55,56].

As shown in Fig. 6(a), the new dielectric functions deviate significantly from those used by Elbaum and Schick [31,32] (up to about 10%). To address the inconsistency between Fiedler *et al.* [57] and Elbaum and Schick [31], we evaluate Casimir-Lifshitz free energies in the ice-water-vapor and water-ice-vapor systems with these new data [see Fig. 6(b)]. The results are clearly in favor of the conclusions in Ref. [57], since an ice film of micron size is promoted by the Casimir-Lifshitz interaction, while the ice-water-vapor configuration is unstable. Therefore it seems that the investigations are converging to similar conclusions as the properties of media are characterized more and more accurately. Further exploring the ice-freezing on silica rocks as in Ref. [36], we see a vastly different picture. As illustrated in Figs. 6(c) and 6(d), with the dielectric functions for silica by Malyi *et al.* [59], if the average cell volume of silica is small enough, for instance
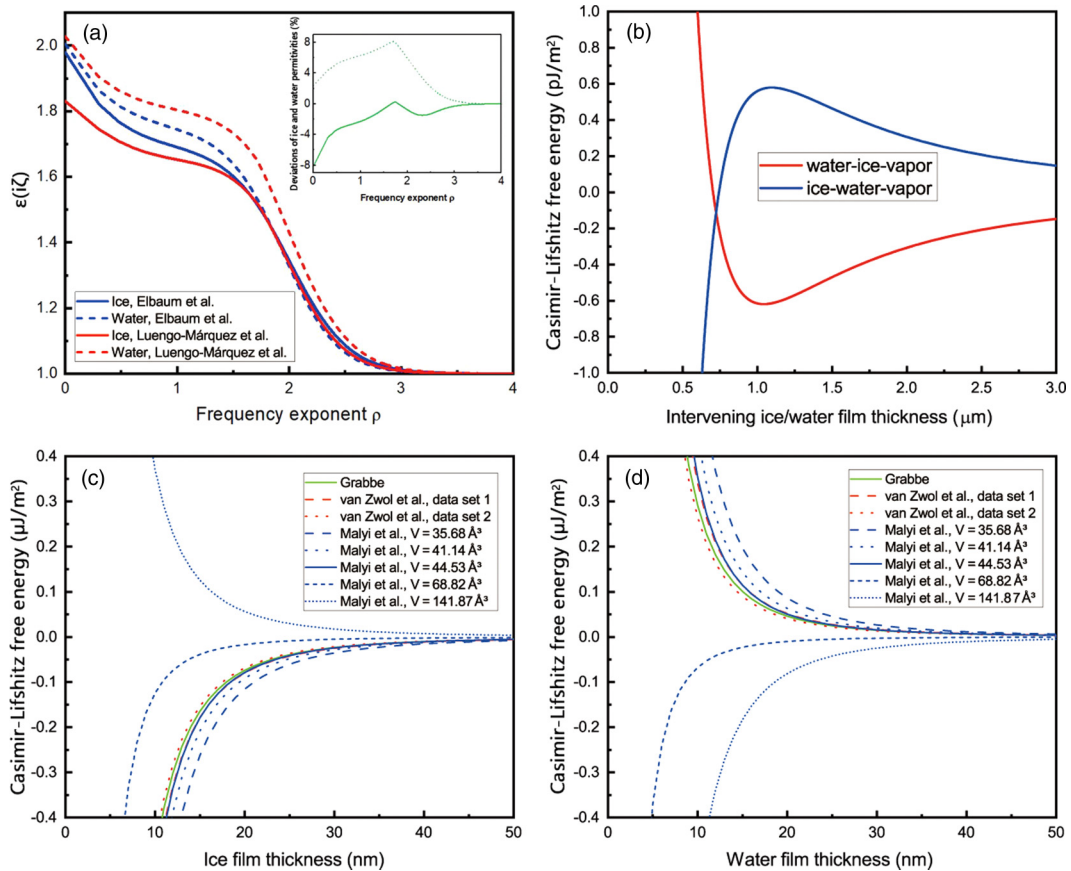
FIG. 6. Previous work revisited with the latest dielectric functions for ice and water [55,56] near the triple point of water. (a) A comparison between the latest dielectric functions [55,56] (LM) and those used by Elbaum and Schick [31,32] (ES). The error between them is defined as $(\varepsilon_{LM} - \varepsilon_{ES})/\varepsilon_{LM}$. The dependence of errors on the frequency exponent ρ for ice (solid green) and water (dashed green) are given in the inset. (b) The Casimir-Lifshitz interaction free energies of ice-water-vapor and water-ice-vapor configurations evaluated with the latest data. Utilizing the new data, (c) and (d) demonstrate the dependence of free energy on ice and water films in the silica-ice-water and silica-water-ice configurations, respectively.

$V = 35.68$ Å^3, the ice film separating this silica and water should vanish to stabilize the system. On the contrary, when the average cell volume V is large, such as $V = 141.87$ Å^3, a nano-sized water film is predicted to vanish. The sensitivity to the average cell volume is particularly striking. For example, for $V = 68.82$ Å^3, as shown in Fig. 6, the material contacting with the surface of this silica can be either ice or water, depending on the initial state. In these three-layer cases, the premelting and formation of ice, characterized by the nano- or micron-sized intervening layer, are not seen with the new data, unlike that claimed before [36]. But the multistable property for some particular case may offer convenience for observations. As for the four-layer cases, drastic modifications caused by the new data are obvious according to Fig. 7. We see one and only one local and global minimum of Casimir-Lifshitz free energy (located at about $d_3 \approx d_2 = 0.2 \mu m$) in Fig. 7(a), instead of two local minima for separated regions as in Fig. 5(a). This is further illustrated by comparing Fig. 7(b) with Fig. 5(b). Furthermore, for the $V = 68.82$ Å^3 silica, Fig. 7(c) and Fig. 5(c) show totally different behaviors. Without a trench as in Fig. 5(c), Fig. 7(c) is more analogous to Fig. 5(e), and the similarities are also found between Fig. 7(d) and Fig. 5(f). The difference between the $V = 68.82$ Å^3 cases in Fig. 5(c) and Fig. 7(c) is that a much deeper basin is found

in Fig. 7(c). For rock built from quartz (the silica that mimics this best in our study is the one with $V = 35.68$ Å^3), we find in Fig. 7(b) a shallow energy minimum as a function of water layer thickness. This minimum moves with increasing total thickness of the ice + water layer indicating growth of the water layer.

IV. DISCUSSION

As is known, the static (zeroth order of Matsubara frequency) terms are quite important to the Casimir-Lifshitz interaction and thus the premelting and formation phenomena. However, as we shall see below, a relative wide band of electromagnetic responses (mainly the electric response here) of materials exerts significant influence as well. An explicit investigation on this effect will not only clarify the physical picture but also be requisite when analyzing or engineering ice premelting and formation processes in realistic and practical systems. Rewrite the Casimir-Lifshitz free energy in Eq. (1) as the sum of the contributions from each Matsubara frequency,
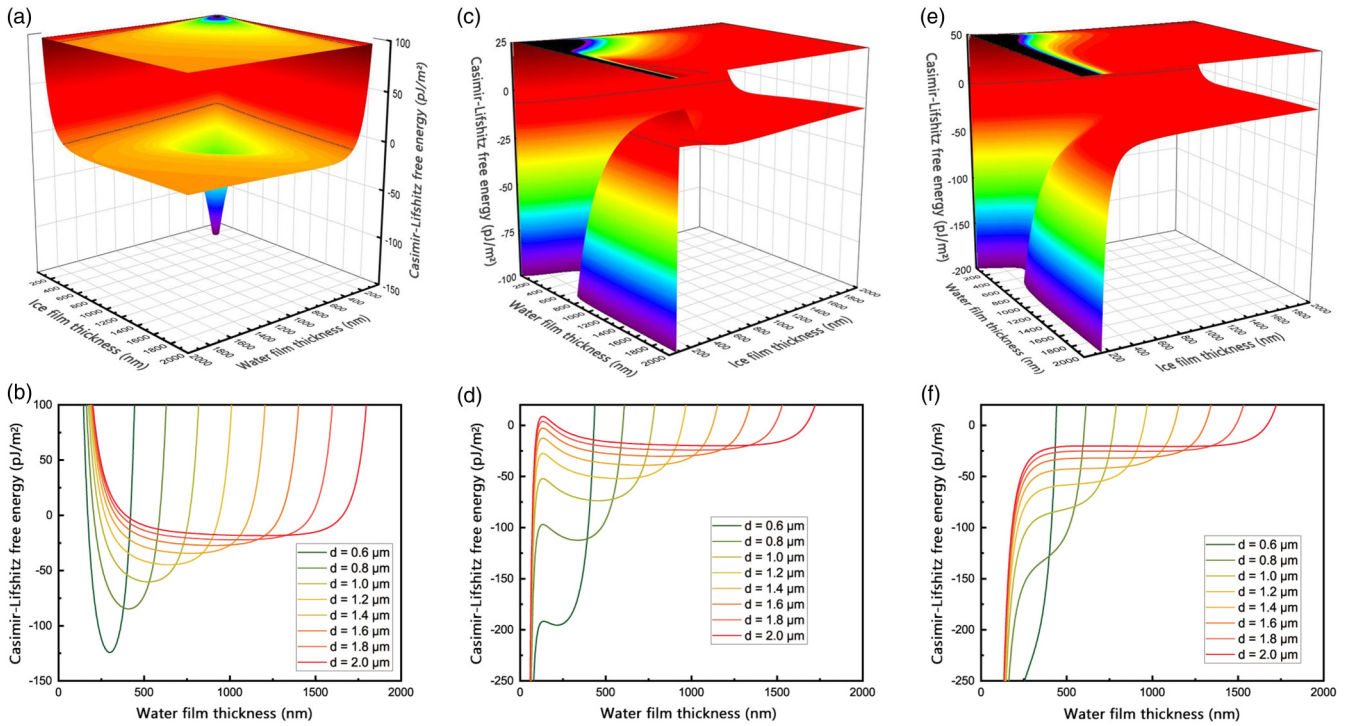
$$F = \sum_{n=0}^{\infty} \Delta F(n), \tag{5}$$

FIG. 7. The Casimir interaction free energy of silica-water-ice-vapor system at $T = 273.16$ K with the average volume per SiO$_2$ being $V = 35.68$ Å^3 (a and b), $V = 68.82$ Å^3 (c and d), and $V = 141.87$ Å^3 (e and f). The latest dielectric functions for ice and water from Luengo-Márquez and MacDowell [55,56] are employed. For subfigures a, c, and e (the corresponding projection of each 3D surface is given at the top), the dependence of free energy on the thicknesses of ice and water films is demonstrated. For subfigures b, d and f, the dependence of free energy as the function of water film thickness, with the total thickness of ice and water layers fixed as $d = d_2 + d_3$, are given.

then with this expression we look into the details of Casimir-Lifshitz free energy as Fig. 8 shows. As demonstrated in Fig. 8(a), for small separations, $\Delta F(n > 0)$ can be large enough to make considerable contributions even in very high orders of Matsubara terms. For instance, when $d = 2.5$ nm, $\Delta F(n)$ can be up to 10% of $|\Delta F(0)|$ even for $n = 125$ and deceases slowly, which renders the total Casimir-Lifshitz free energy large and positive. When the thickness is large, such as $d = 20.0$ nm in the same figure, for high orders $\Delta F(n)$ remains close to zero. The minimum of Casimir-Lifshitz free energy in Fig. 3 is accomplished since the negative Matsubara terms are also suppressed by large separations. So in this case, the properties of dielectric functions in the midinfrared to UV region are the most important. To understand the connection between the dielectric properties and the behaviors in Fig. 8(a), we introduce the following characteristic index

$$\eta = A\frac{(\varepsilon_3 - \varepsilon_2)(\varepsilon_2 - \varepsilon_1)}{\varepsilon_2}, \qquad (6)$$

in which an arbitrary constant factor A for each system, independent of the properties of media, is added. Then according to Fig. 8(a) and especially Fig. 8(b), the correspondence between $\Delta F(n)$ and η is straightforward, which facilitates the prediction for the stability properties due to Casimir-Lifshitz interaction. Both Fig. 8(a) and Fig. 8(b) justify the outstanding contribution from the zeroth Matsubara term, and both nonretarded and retarded interactions are important. Typically the relation $\sqrt{\varepsilon_2(i\zeta)}\zeta d \sim 1$ could be useful when estimating

the size of intermediate medium if any. The correspondence between $\Delta F(n)$ and η is also evidently illustrated by Fig. 8(d). A particularly novel situation, introduced by the latest data for ice and water [55,56], is the $V = 68.82$ Å^3 case depicted in Fig. 6. Figure 8(c) shows that either for silica-ice-water or for silica-water-ice, $\Delta F(n)$ in the $V = 68.82$ Å^3 case is always negative, which is due to negative (but close to zero) characteristic indices for either case. The characteristic index η (and that for four-layer cases) could serve as a tool to search on systems for experimental studies or applications, which should exhibit specific ice premelting or formation properties. For instance, one would like the characteristic index of the system to properly change sign in the band of frequency if a premelting water layer or partially freezing ice layer is required. To be more specific, a sign change happens at the frequency about 10 PHz as shown in Fig. 8(b) for $V = 35.68$ Å^3 case, leading to a thin ice film stabilized by the Casimir-Lifshitz interaction. A similar behavior but with opposite sign for $V = 141.87$ Å^3 case in Fig. 8(b) will destabilize this film, if any.

The four-layer scenarios are much more complex. But we see a clear pattern in Fig. 5 and Fig. 7, and the competition among the three interaction terms should be responsible for it. Before we discuss this issue, it is helpful to see how the four-layer system is changed to a three-layer case. To be more specific, we focus on the systems investigated in Fig. 7, which leads us to the results in Fig. 9. There, for each given thickness of the water layer, we consider the minimum Casimir-Lifshitz free energy reached by varying the thickness of ice layer.
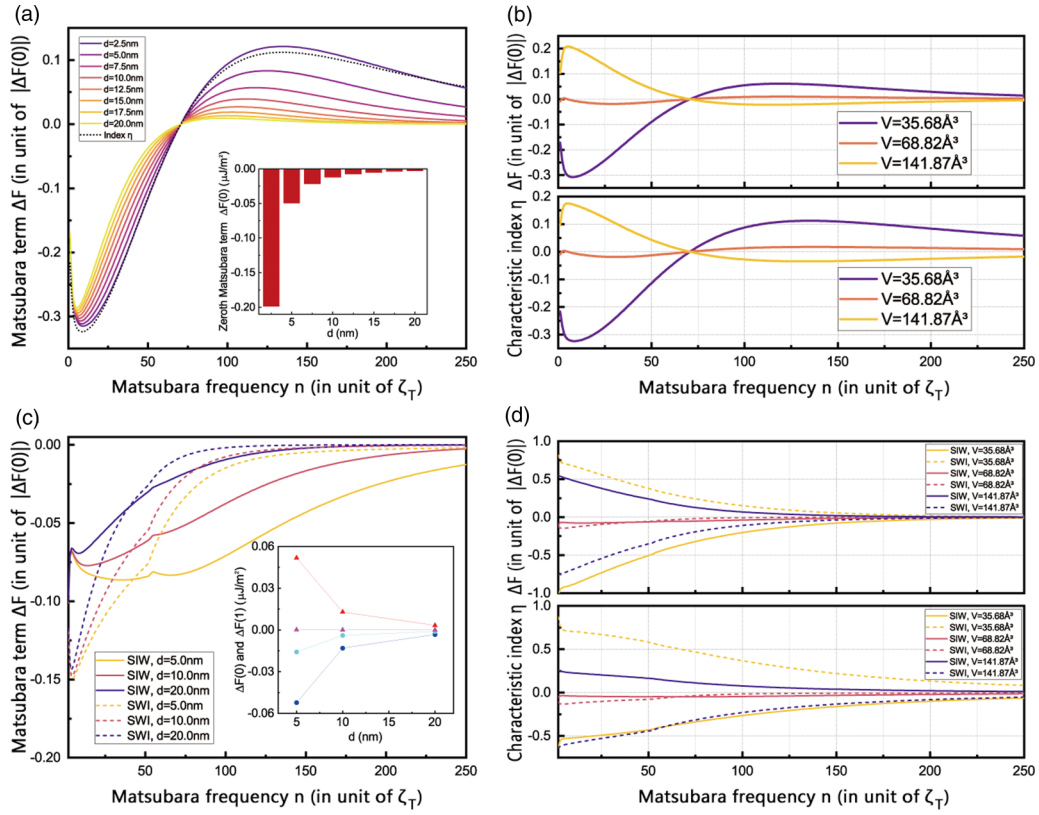
FIG. 8. The contribution from Matsubara terms $\Delta F(n)$ and the characteristic indices η for silica-ice-water (SIW) in Fig. 3 (a and b) and both silica-ice-water and silica-water-ice (SWI) in Figs. 6(c) and 6(d). (a) The nonzero Matsubara terms $\Delta F(n), n \geqslant 1$ defined in Eq. (5) normalized by $|\Delta F(0)|$ when the average cell volume of the silica is $V = 35.68$ Å^3. (b) A comparison between $\Delta F(n)$ and the characteristic index η defined in Eq. (6) with $d = 7.0$ nm fixed. (c) The Matsubara terms $\Delta F(n)$ defined in Eq. (5) normalized by $|\Delta F(0)|$ when the average cell volume of the silica is $V = 68.82$ Å^3. The zeroth (silica-ice-water, blue circle; silica-water-ice, red triangle) and first (silica-ice-water, cyan circle; silica-water-ice, magenta triangle) order are given in the inset. (d) A comparison between $\Delta F(n)$ and the characteristic index η defined in Eq. (6) with $d = 10.0$ nm fixed.

Denote the contributions to the free energy from silica-water-ice, water-ice-vapor, and silica-vapor as F_{SWI}, F_{WIV}, and F_{14} respectively, corresponding to 1-2-3, 2-3-4 DLP systems and F_{14} described in Eq. (4), then we use the ratios defined as

$$\beta_{\text{SWI}} = \frac{F_{\text{WIV}}}{F_{\text{SWI}}}, \quad \beta_{14} = \frac{F_{\text{WIV}}}{F_{14}}, \tag{7}$$

which are demonstrated in Fig. 9. As one increases the given thickness of water layer, the contributions from F_{SWI} and F_{14} are both suppressed. It is absolutely natural since with an enlarged separation between silica and ice, and hence silica and vapor, the interaction between these two materials will surely decay. Then only the water-ice-vapor interaction survives, which is illustrated as the consistency between the inset of Fig. 9 and Fig. 6(b). More importantly, Fig. 9 shows that when the thickness of the water layer is not so large, the Casimir-Lifshitz interaction between silica and vapor dominates, which is clearly shown in Fig. 9 with relatively small water layer thickness. Therefore the interactions mediated by more than one medium can be much more significant than the classical DLP contributions, even with larger separations. This is further confirmed by observing that F_{SWI} decays much faster than F_{14} as a larger water layer thickness is given.

For the Casimir-Lifshitz interaction mediated by two media, one might expect that its free energy in this case here,

namely, F_{14}, could be characterized by the index as in Eq. (6), that is, from Eq. (4),

$$\eta \propto \tilde{r}_{43}\left(1 - \tilde{r}_{32}^2\right)\tilde{r}_{21}, \quad \tilde{r}_{ij} = \frac{\varepsilon_j - \varepsilon_i}{\varepsilon_j + \varepsilon_i}. \tag{8}$$

Equation (8) includes the direct interaction between silica-water (or 1-2) and ice-vapor (or 3-4) interfaces and the leading contribution passing through the water-ice (or 2-3) interface once. However, although one can check that contributions from interactions mediated by a third interface are quite small compared with the direct interaction, namely, the $O(r_{43}^s r_{21}^s)$ term in Eq. (4) or $\tilde{r}_{43}\tilde{r}_{21}$ in the characterized form, Fig. 10 shows that the characteristic index defined in Eq. (8) is not enough in this case. As the Matsubara frequency increases, the Matsubara term and its corresponding characteristic index η (red triangle) behave distinctly different. This actually illustrates the fact that properties of materials can strongly influence the effective range of Casimir-Lifshitz interaction. Unlike in Fig. 8, the interaction range in the four-layer case here is of micron size order, almost one thousand times larger than that in Fig. 8. It is thus reasonable to include the contribution from the retardation effect, which leads us to a modified characteristic index, defined as follows:

$$\tilde{\eta} \propto \tilde{r}_{43}\left(1 - \tilde{r}_{32}^2\right)\tilde{r}_{21}e^{-2(\sqrt{\varepsilon_2}d_2 + \sqrt{\varepsilon_3}d_3)\zeta}. \tag{9}$$
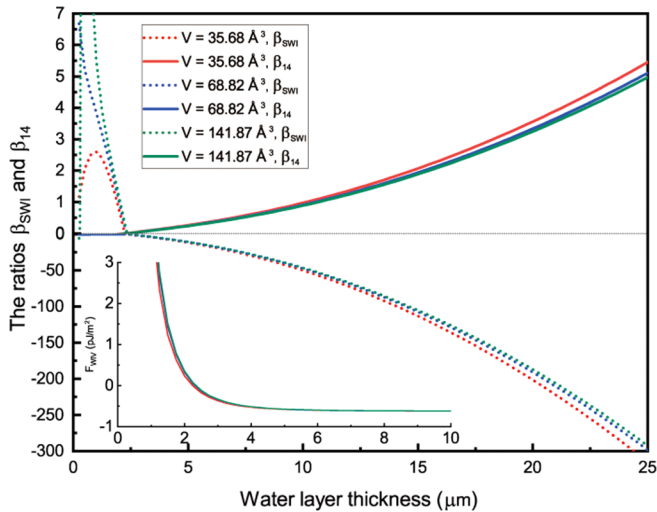
FIG. 9. The contributions from different Casimir-Lifshitz interactions to the minimum free energies with different given water layer thicknesses. The systems investigated in Fig. 7 are studied in detail. The contributions from F_{SWI} and F_{14} are shown in terms of β_{SWI} and β_{14} defined in Eq. (7). In the inset, the corresponding free energy of water-ice-vapor configuration is given.

In Fig. 10, $\widetilde{\eta}$ (blue circle) proves itself a good characteristic index for the Casimir-Lifshitz free energy mediated by more than one layer at least for F_{14} in Eq. (3). So both properties of the materials and the retardation of the field (in addition to the static interaction) exert significant influences. The minimum of the total Casimir-Lifshitz free energy is obtained due to a subtle balance among those various factors above, which show themselves in each contributing free energies no matter whether they arise from three- or four-layer cases. The Casimir-Lifshitz interaction is many body in nature after all.

Though complicated, we could also try to understand some of the details of this subtle balance from both Fig. 5 and Fig. 7,
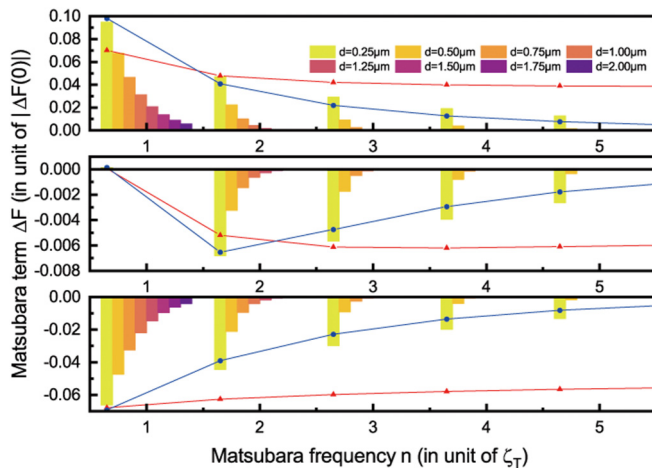

FIG. 10. The Matsubara term as a function of the sum d of the water d_2 and ice d_3 thickness with $d = 2d_2$. The systems investigated in Fig. 7 are studied in detail. Red triangles and blue circles are, respectively, plotted with overall scale adjusted for characteristic indices η and $\widetilde{\eta}$ defined in Eq. (8) and Eq. (9), with $d = 2d_2 = 0.25\ \mu$m.
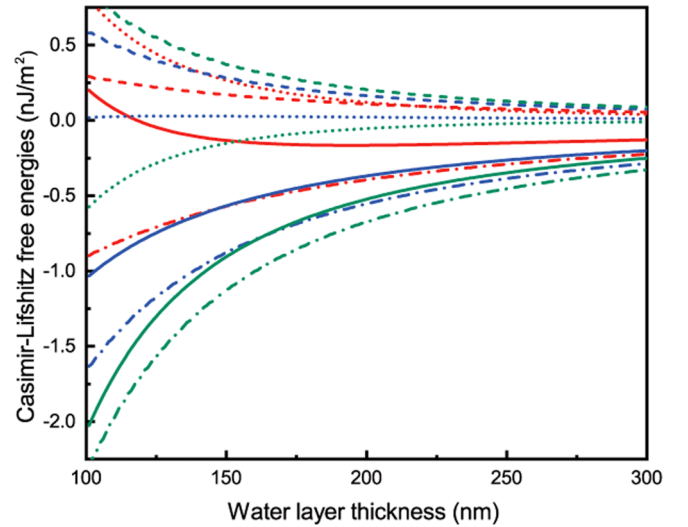

FIG. 11. The systems investigated in Fig. 7 are studied in detail. For different silica materials with the average cell volume $V = 35.68\ \text{Å}^3$ (red), $V = 68.82\ \text{Å}^3$ (blue), and $V = 141.87\ \text{Å}^3$ (green), the Casimir-Lifshitz free energies from silica-water-ice F_{SWI} (dot), water-ice-vapor F_{WIV} (dash), four-layer interaction F_{14} (dash dot), and the total free energy $F = F_{SWI} + F_{WIV} + F_{14}$ (solid) are plotted when the minimum of F is reached for each given water layer thickness.

in which a clear pattern presents, though they look complex at first glance. Figure 5(a) obviously gains its two trenches corresponding to the minima of Casimir-Lifshitz free energies for silica-ice-water and ice-water-vapor evaluated with the data in previous work [36]. The similarities between Figs. 5(c) and 5(e) and Figs. 7(a) and 7(c) are also apparent. For simplicity, we focus on the systems depicted by Fig. 7 again. According to Fig. 11, for the silica material with the average cell volume $V = 35.68\ \text{Å}^3$, both silica-water-ice F_{SWI} and water-ice-vapor F_{WIV} contribute positively when the thickness of the water layer is given in the range 100 nm $< d_2 <$ 300 nm. On the contrary, F_{14} is always negative, and together F_{SWI} and F_{WIV} produce a global minimum of total Casimir-Lifshitz free energy at about $d_2 \approx 0.2\ \mu$m, just as shown in Fig. 7(a). Larger average cell volume decreases the permittivity of silica material, which not only renders F_{14} more negative but also eliminates the ability of F_{SWI} to compensate F_{14}. So the behaviors shown in Figs. 7(c) and 7(e) are mainly caused by F_{14} (also see the $V = 68.82\ \text{Å}^3$ and $V = 141.87\ \text{Å}^3$ cases in Fig. 11). Based on these analyses, it can be expected that with the characteristic indices for DLP and four-layer interactions defined above, the possible influences of Casimir-Lifshitz interaction on the stability of a configuration under study can be predicted qualitatively.

V. CONCLUSIONS

In this paper, we redo and extend the previous work on the premelting and formation of ice either on a bulk of silica rock or on ice-cold water, caused by the Casimir-Lifshitz interaction. It can be safely claimed that the detailed properties of materials (in the cases considered in this paper, their permittivities) influence these premelting and formation phenomena.

(During our study, a mistake in our previous work [36] has been spotted and the corrected results are given.) Perhaps the most important observation from the recent modeling of ice and water could be that their dielectric functions at the triple point of water only have crossings between the $n = 0$ and the $n = 1$ Matsubara frequencies [55–57]. This fundamentally alters the predicted behavior compared when the dielectric functions from Elbaum and Schick are used [31]. For the original ice-water-vapor structure, the most recent dielectric functions for ice and water lead to the formation of a thin ice layer on the water, which is in contradiction with the premelting prediction from Elbaum and Schick [31]. Our results confirm those in Ref. [57], that is, a micron-sized ice layer forms on the surface of cold water. We suggest that careful optical measurements of water and ice at different temperatures and pressures should be highly interesting. Such measurements have the potential to improve our understanding of the role for dispersion forces in ice formation and melting.

As can be expected, the three-layer silica-ice-water and four-layer silica-ice-water-vapor systems behave differently from those studied in previous work using the parameters from Elbaum and Schick. [31–37,61]. The ice formation on the silica is not seen, but a bulk of ice or water is directly in contact with the silica surface, depending on the permittivity of the particular silica materials or the initial condition of ice or water for some cases, such as the $V = 68.82$ Å^3 case here.

In four-layer scenarios, we see both a single global stable state of water and ice layers [Fig. 5(c) and Fig. 7(a)], the coexistence of a metastable and a stable state [Fig. 5(a)], and the relatively stable region like a waterfall [Fig. 5(e) and Figs. 7(c) and 7(e)]. Those complicated situations occur due to correlations of different types of Casimir-Lifshitz interactions. Two indices are introduced to characterize those interactions here for the four-layer case. With the characteristic indices, it will be easier to estimate influences of the Casimir-Lifshitz interaction on the stability of the system to be investigated. On the theoretical side, they and their generalizations in more complex situations, for instance, multislab cases in general, may help to throw light on the mechanics of the Casimir-Lifshitz interaction mediated by inhomogeneous materials, which is now still largely veiled.

In this work we have analyzed the induced inhomogeneous free energies in layered media generated by Casimir-Lifshitz interactions. This analysis assumes that surface charge and surface adsorption of free ions (salt or dissociated water) is not significant, corresponding to a system at the isoelectric point (IEP) where any such surface charge is neutralized. Both ice [74] and quartz (silica [75]) have a low IEP around pH 3–3.5. At other pH conditions away from the IEP, including pH 7, charge-dependent effects can be important [39], with ion adsorption layers generally creating a repulsive force that would enhance premelting. These charge-induced interactions deserve further attention and must in general be important for both ice formation and premelting.

APPENDIX: DERIVATION OF FREE ENERGY FOR FOUR-SLAB SYSTEM

We consider a four-layer system, each layer being homogeneous:

$$
\varepsilon, \mu(z) = \begin{cases}
z < a : & \epsilon_1, \mu_1, \\
a < z < b : & \epsilon_2, \mu_2, \\
b < z < c : & \epsilon_3, \mu_3, \\
c < z : & \epsilon_4, \mu_4.
\end{cases} \tag{A1}
$$

The free energy is given in general by

$$
F = \frac{T}{2} \sum_{n=-\infty}^{\infty} \int \frac{d^2k}{(2\pi)^2} \ln \Delta^E \Delta^H, \tag{A2}
$$

the sum being over Matsubara frequencies ζ_n. We will use the inhomogeneous medium description given in Ref. [58]. We regard the regions 2 and 3 as a single region, called "in" where the medium is inhomogeneous. To obtain an unambiguously finite result, we subtract a reference energy corresponding to removing the boundary a, that is, letting medium 2 to extend to $-\infty$. Then, we add back in the energy corresponding to that reference energy. So

$$
F = F_{\text{sub}} + F_{\text{ref}}. \tag{A3}
$$

Here we consider the TE contribution only, the TM contribution being obtained by the obvious substitutions.

Consider first the reference situation, which is just the familiar DLP configuration. There, according to Ref. [58]

$$
\Delta_{\text{ref}}^E = 1 - \frac{[e_{2,-}, e_{3,-}]_\mu(b)[e_{3,+}, e_{4,+}]_\mu(c)}{[e_{2,-}, e_{3,+}]_\mu(b)[e_{3,-}, e_{4,+}]_\mu(c)}, \tag{A4}
$$

where e_i satisfies

$$
\left(\partial_z \frac{1}{\mu_i} \partial_z - \frac{k^2}{\mu_i} - \varepsilon_i \zeta^2 \right) e_i = 0, \tag{A5}
$$

in which the medium i has been analytically extended to the whole space. The generalized Wronskians are defined by (prime means derivative with respect to the argument)

$$
[e_i, e_j] = \frac{1}{\mu_i} e_i' e_j - \frac{1}{\mu_j} e_j' e_i, \tag{A6}
$$

evaluated at the same point.

In the DLP configuration, we may define

$$
e_{i,\pm} = e^{\mp \kappa_i z}, \quad \kappa_i = \sqrt{k^2 + \epsilon_i \mu_i \zeta^2}. \tag{A7}
$$

Then it is immediate to find

$$
\Delta_{\text{ref}}^E = 1 - r_{23}^E r_{43}^E e^{-2\kappa_3(c-b)}, \tag{A8}
$$

in terms of the reflection coefficients

$$
r_{ij}^E = \frac{\hat{\kappa}_j - \hat{\kappa}_i}{\hat{\kappa}_j + \hat{\kappa}_i}, \quad \hat{\kappa}_i = \frac{\kappa_i}{\mu_i}. \tag{A9}
$$

This directly gives the Lifshitz energy in Eq. (1).

Now for the subtracted four-slab configuration, we need to compute

$$\Delta^E_{\rm sub} = 1 - \frac{[e_{1,-}, e_{{\rm in},-}]_\mu(a)[e_{{\rm in},+}, e_{4,+}]_\mu(c)}{[e_{1,-}, e_{{\rm in},+}]_\mu(a)[e_{{\rm in},-}, e_{4,+}]_\mu(c)}, \qquad {\rm (A10)}$$

where the effort is only in finding the solution in the $2 + 3$ region. We can take $e_{{\rm in}\mp}(z)$ to be $e^{\pm\kappa_2 z}$ for $a < z < b$; then by requiring, from the differential equation Eq. (A5), continuity of the solution, and of $\frac{1}{\mu}$ times the derivative of the solution, we find

$$e_{{\rm in},\mp} = e^{\pm\kappa_2 z}, \ a < z < b \qquad {\rm (A11a)}$$

$$e_{{\rm in},\mp}(z) = [(\hat\kappa_3 - \hat\kappa_2)e^{\mp\kappa_3(z-b)} + (\hat\kappa_3 + \hat\kappa_2)e^{\pm\kappa_3(z-b)}]$$

$$\times \frac{1}{2\hat\kappa_3}e^{\pm\kappa_2 b}, \ b < z < c. \qquad {\rm (A11b)}$$

Then $\Delta^E_{\rm sub}$ is readily calculated to be

$$\Delta^E_{\rm sub} = 1 + r^E_{12} e^{-2\kappa_2(b-a)} \frac{r^E_{23} e^{2\kappa_3(c-b)} + r^E_{34}}{e^{2\kappa_3(c-b)} + r^E_{34} r^E_{23}}. \qquad {\rm (A12)}$$

When this is multiplied by $\Delta^E_{\rm ref}$ in Eq. (A8), the denominator in Eq. (A12) is canceled, and we are left with

$$\Delta^E = 1 + r^E_{43} r^E_{32} e^{-2\kappa_3(c-b)} + r^E_{32} r^E_{21} e^{-2\kappa_2(b-a)}$$

$$+ r^E_{21} r^E_{43} e^{-2\kappa_2(b-a)} e^{-2\kappa_3(c-b)}, \qquad {\rm (A13)}$$

which is precisely the result stated in Eq. (4) after we replace $b - a \to d_2$, $c - b \to d_3$. The decomposition given in Section II of $F = F_{14} + F_{13} + F_{24}$, is now immediate, where F_{14} has a rather immediate interpretation in terms of multiple scattering, given that the transmission coefficient between region 2 and 3 satisfies $t^2_{23} = 1 - r^2_{23}$.

[1] H. B. G. Casimir, On the attraction between two perfectly conducting plates, Proc. Kon. Ned. Akad. Wetensch. **51**, 793 (1948).

[2] E. M. Lifshitz, The theory of molecular attractive forces between solids, Sov. Phys. JETP **2**, 73 (1956).

[3] I. E. Dzyaloshinskii, E. M. Lifshitz, and L. P. Pitaevskii, The general theory of van der Waals forces, Adv. Phys. **10**, 165 (1961).

[4] D. Tabor and R. H. S. Winterton, The direct measurement of normal and retarded van der Waals forces, Proc. Roy. Soc. **312**, 435 (1969).

[5] J. N. Israelachvili and D. Tabor, The measurement of van der Waals dispersion forces in the range 1.5 to 130 nm, Proc. Roy. Soc. A **331**, 19 (1972).

[6] L.R. White, J. N. Israelachvili, and B. W. Ninham, The dispersion interaction of crossed mica cylinders, J. Chem. Soc. Faraday Trans. I **72**, 2526 (1976).

[7] C. H. Anderson and E. S. Sabisky, Phonon Interference in Thin Films of Liquid Helium, Phys. Rev. Lett. **24**, 1049 (1970).

[8] F Hauxwell and R.H Ottewill, A study of the surface of water by hydrocarbon adsorption, J. Colloid Interface Sci. **34**, 473 (1970).

[9] E. S. Sabisky and C. H. Anderson, Verification of the Lifshitz theory of the van der Waals potential using liquid-helium films, Phys. Rev. A **7**, 790 (1973).

[10] V. A. Parsegian and B. W. Ninham, Application of the Lifshitz theory to the calculation of van der Waals forces across thin lipid films, Nature (London) **224**, 1197 (1969).

[11] B. W. Ninham and V. A. Parsegian, Van der Waals forces: special characteristics in lipid-water systems and a general method of calculation based on the Lifshitz theory, Biophys. J. **10**, 646 (1970).

[12] P. Richmond and B. W. Ninham, Calculations, using Lifshitz theory, of the height vs. thickness for vertical liquid helium films, Solid State Commun. **9**, 1045 (1971).

[13] P. Richmond and B. W. Ninham, A note on the extension of the Lifshitz theory of van der Waals forces to magnetic media, J. Phys. C: Solid State Phys. **4**, 1988 (1971).

[14] B. W. Ninham, B. V. Derjaguin and J. Theo. G. Overbeek. Their times, and ours, Substantia **3**, 65 (2019).

[15] S. K. Lamoreaux, Demonstration of the Casimir Force in the 0.6 to 6 μm Range, Phys. Rev. Lett. **78**, 5 (1997).

[16] S. K. Lamoreaux, Erratum: Demonstration of the Casimir Force in the 0.6 to 6 μm Range [Phys. Rev. Lett. **78**, 5 (1997)], Phys. Rev. Lett. **81**, 5475(E) (1998).

[17] A. O. Sushkov, W. J. Kim, D. A. R. Dalvit, and S. K. Lamoreaux, Observation of the thermal Casimir force, Nat. Phys. **7**, 230 (2011).

[18] G. L. Klimchitskaya and V. M. Mostepanenko, Recent measurements of the Casimir force: Comparison between experiment and theory, Mod. Phys, Lett. A **35**, 2040007 (2020).

[19] M. Liu, Y. Zhang, G. L. Klimchitskaya, V. M. Mostepanenko, and U. Mohideen, Experimental and theoretical investigation of the thermal effect in the Casimir interaction from graphene, Phys. Rev. B **104**, 085436 (2021).

[20] G. Bimonte, B. Spreng, P. A. Maia Neto, G.-L. Ingold, G. L Klimchitskaya, V. M. Mostepanenko, and R. S. Decca, Measurement of the Casimir force between 0.2 and 8 μm: Experimental procedures and comparison with theory, Universe **7**, 93 (2021).

[21] M. Boström and B. E. Sernelius, Thermal effects on the Casimir Force in the 0.1–5 μm Range, Phys. Rev. Lett. **84**, 4757 (2000).

[22] I. Brevik, S. A. Ellingsen, and K. A. Milton, Thermal corrections to the Casimir effect, New J. Phys. **8**, 236 (2006).

[23] I. Brevik and J. S. Høye, Temperature dependence of the Casimir force, Eur. J. Phys. **35**, 015012 (2013).

[24] G. L. Klimchitskaya and V. M. Mostepanenko, Casimir free energy of dielectric films: Classical limit, low-temperature behavior and control, J. Condens. Matter Phys. **29**, 275701 (2017).

[25] B. E. Sernelius, *Fundamentals of van der Waals and Casimir Interactions*, Springer Series on Atomic, Optical, and Plasma Physics (Springer, Cham, Switzerland, 2018), Vol. 102.

[26] K. A. Milton, *The Casimir Effect: Physical Manifestations of Zero-Point Energy* (World Scientific, Singapore, 2001).

[27] M. Bordag, G. L. Klimchitskaya, U. Mohideen, and V. M. Mostepanenko, *Advances in the Casimir Effect* (Oxford Science Publications, Oxford, 2009).

[28] D. Dalvit, P. Milonni, D. Roberts, and F. da Rosa, *Casimir Physics*, Lecture Notes in Physics (Springer, Berlin, Heidelberg, 2011), Vol. 834.

[29] S. Y. Buhmann, *Dispersion Forces I: Macroscopic quantum electrodynamics and ground-state Casimir, Casimir–Polder and van der Waals forces*, Springer Tracts in Modern Physics (Springer, Berlin, Heidelberg, 2013), Vol. 247.

[30] S. Y. Buhmann, *Dispersion Forces II: Many-Body Effects, Excited Atoms, Finite Temperature and Quantum Friction*, Springer Tracts in Modern Physics (Springer, Berlin, Heidelberg, 2013), Vol. 248.

[31] M. Elbaum and M. Schick, Application of the Theory of Dispersion Forces to the Surface Melting of Ice, Phys. Rev. Lett. **66**, 1713 (1991).

[32] M. Elbaum and M. Schick, On the failure of water to freeze from its surface, J. Phys. I: France **1**, 1665 (1991).

[33] L. A. Wilen, J. S. Wettlaufer, M. Elbaum, and M. Schick, Dispersion-force effects in interfacial premelting of ice, Phys. Rev. B **52**, 12426 (1995).

[34] P. Thiyam, E. R. A. Lima, O. I. Malyi, D. F. Parsons, S. Y. Buhmann, C. Persson, and M. Boström, Effects of van der Waals forces and salt ions on the growth of water films on ice and the detachment of CO_2 bubbles, Europhys. Lett. **113**, 43002 (2016).

[35] M. Boström, O. I. Malyi, P. Thiyam, K. Berland, I. Brevik, C. Persson, and D. F. Parsons, The influence of Lifshitz forces and gas on premelting of ice within porous materials, Europhys. Lett. **115**, 13001 (2016).

[36] M. Boström, O. I. Malyi, P. Parashar, K. V. Shajesh, P. Thiyam, K. A. Milton, C. Persson, D. F. Parsons, and I. Brevik, Lifshitz interaction can promote ice growth at water-silica interfaces, Phys. Rev. B **95**, 155422 (2017).

[37] P. Parashar, K. V. Shajesh, K. A. Milton, D. F. Parsons, I. Brevik, and M. Boström, Role of zero point energy in promoting ice formation in a spherical drop of water, Phys. Rev. Research **1**, 033210 (2019).

[38] J. S. Wettlaufer, Impurity Effects in the Premelting of Ice, Phys. Rev. Lett. **82**, 2516 (1999).

[39] P. Thiyam, J. Fiedler, S. Y. Buhmann, C. Persson, I. Brevik, M. Boström, and D. F. Parsons, Ice particles sink below the water surface due to a balance of salt, van der Waals, and buoyancy forces, J. Phys. Chem. C **122**, 15311 (2018).

[40] J. G. Dash, Surface melting, Cont. Phys. **30**, 89 (1989).

[41] M. Elbaum, S.G. Lipson, and J.G. Dash, Optical study of surface melting on ice, J. Crys. Growth **129**, 491 (1993).

[42] J. G. Dash, H. Fu, and J. S. Wettlaufer, The premelting of ice and its environmental consequences, Rep. Prog. Phys. **58**, 115 (1995).

[43] J. G. Dash, A. W. Rempel, and J. S. Wettlaufer, The physics of premelted ice and its geophysical consequences, Rev. Mod. Phys. **78**, 695 (2006).

[44] H. Li, M. Bier, J. Mars, H. Weiss, A. Dippel, O. Gutowski, V. Honkimäki, and M. Mezger, Interfacial premelting of ice in nano composite materials, Phys. Chem. Chem. Phys. **21**, 3734 (2019).

[45] J. Benet, P. Llombart, E. Sanz, and L. G. MacDowell, Premelting-Induced Smoothening of the Ice-Vapor Interface, Phys. Rev. Lett. **117**, 096101 (2016).

[46] J. Benet, P. Llombart, E. Sanz, and L. G. MacDowell, Structure and fluctuations of the premelted liquid film of ice at the triple point, Mol. Phys. **117**, 2846 (2019).

[47] L. A. Wilen and J. G. Dash, Frost Heave Dynamics at a Single Crystal Interface, Phys. Rev. Lett. **74**, 5076 (1995).

[48] M. B. Baker and J. G. Dash, Charge transfer in thunderstorms and the surface melting of ice, J. Crys. Growth **97**, 770 (1989).

[49] J. G. Dash and J. S. Wettlaufer, The surface physics of ice in thunderstorms, Can. J. Phys. **81**, 201 (2003).

[50] S. C. Sherwood, V. T. J. Phillips, and J. S. Wettlaufer, Small ice crystals and the climatology of lightning, Geophys. Res. Lett. **33**, L05804 (2006).

[51] S. Kamata, F. Nimmo, Y. Sekine, K. Kuramoto, N. Noguchi, J. Kimura, and A. Tani, Pluto's ocean is capped and insulated by gas hydrates, Nat. Geosci. **12**, 407 (2019).

[52] V. Muñoz-Iglesias and O. Prieto-Ballesteros, Thermal properties of the H_2O-CO_2-Na_2CO_3/CH_3OH/NH_3 systems at low temperatures and pressures up to 50 MPa, ACS Earth Space Chem. **5**, 2626 (2021).

[53] M. Boström, R. W. Corkery, E. R. A. Lima, O. I. Malyi, S. Y. Buhmann, C. Persson, I. Brevik, D. F. Parsons, and J. Fiedler, Dispersion forces stabilize ice coatings at certain gas hydrate interfaces that prevent water wetting, ACS Earth Space Chem. **3**, 1014 (2019).

[54] M. Boström, V. Esteso, J. Fiedler, I. Brevik, S. Y. Buhmann, C. Persson, S. Carretero-Palacios, D. F. Parsons, and R. W. Corkery, Self-preserving ice layers on CO_2 clathrate particles: implications for Enceladus, Pluto and similar ocean worlds, Astron. Astrophys. **650**, A54 (2021).

[55] J. Luengo-Márquez and L. G. MacDowell, Lifshitz theory of wetting films at three phase coexistence: The case of ice nucleation on Silver Iodide (AgI), J. Colloid Interface Sci. **590**, 527 (2021).

[56] J. Luengo-Márquez and L. G. MacDowell, private communication (2021).

[57] J. Fiedler, M. Boström, C. Persson, I. H. Brevik, Robert W. Corkery, S. Y. Buhmann, and D. F. Parsons, Full-spectrum high resolution modeling of the dielectric function of water, J. Phys. Chem. B **124**, 3103 (2020).

[58] Y. Li, K. A. Milton, X. Guo, G. Kennedy, and S. A. Fulling, Casimir forces in inhomogeneous media: Renormalization and the principle of virtual work, Phys. Rev. D **99**, 125004 (2019).

[59] O. I. Malyi, M. Boström, V. V. Kulish, P. Thiyam, D. F. Parsons, and C. Persson, Volume dependence of the dielectric properties of amorphous SiO_2, Phys. Chem. Chem. Phys. **18**, 7483 (2016).

[60] P. J. van Zwol and G. Palasantzas, Repulsive Casimir forces between solid materials with high-refractive-index intervening liquids, Phys. Rev. A **81**, 062502 (2010).

[61] V. Esteso, S. Carretero-Palacios, L. G. MacDowell, J. Fiedler, D. F. Parsons, F. Spallek, H. Míguez, C. Persson, S. Y. Buhmann, I. Brevik *et al.*, Premelting of ice adsorbed on a rock surface, Phys. Chem. Chem. Phys. **22**, 11362 (2020).

[62] A Grabbe, Double layer interactions between silylated silica surfaces, Langmuir **3**, 797 (1993).

[63] P. Parashar, K. A. Milton, Y. Li, H. Day, X. Guo, S. A. Fulling, and I. Cavero-Peláez, Quantum electromagnetic stress tensor in an inhomogeneous medium, Phys. Rev. D **97**, 125009 (2018).

[64] J. N. Munday, F. Capasso, and V. A. Parsegian, Measured long-range repulsive Casimir-Lifshitz forces, Nature (London) **457**, 170 (2009).

[65] I. Brevik, Fluids in electric and magnetic fields: Pressure variation and stability, Can. J. Phys. **60**, 449 (1982).

[66] L. D. Landau and E. M. Lifshitz, *Electrodynamics of Continuous Media* (Pergamon Press, Oxford, 1960).

[67] A. I. Volokitin, Electric double layer effect in an extreme near-field heat transfer between metal surfaces, Phys. Rev. B **103**, L041403 (2021).

[68] A. I. Volokitin, Enhancement of non-contact friction between metal surfaces induced by the electrical double layer, Appl. Surf. Sci. **6**, 100160 (2021).

[69] R. A. Robinson and R. H. Stokes, *Electrolyte Solutions*, 2nd ed. (Butterworths Scientific Publications, London, 1959).

[70] A. I. Volokitin, Effect of an electric field in the heat transfer between metals in the extreme near field, JETP Lett. **109**, 749 (2019).

[71] A. I. Volokitin and B. N. J. Persson, Electric field effect in heat transfer in 2D devices, J. Condens. Matter Phys. **32**, 255301 (2020).

[72] J. Daniels, Bestimmung der optischen konstanten von eis aus energie-verlustmessungen von schnellen elektronen, Opt. Commun. **3**, 240 (1971).

[73] M. Seki, K. Kobayashi, and J. Nakahara, Optical spectra of hexagonal ice, J. Phys. Soc. Jpn. **50**, 2643 (1981).

[74] N. Kallay, A. Čop, E. Chibowski, and L. Holysz, Reversible charging of the ice-water interface: II. Estimation of equilibrium parameters, J. Colloid Interface Sci. **259**, 89 (2003).

[75] P. G. Hartley, I. Larson, and P. J. Scales, Electrokinetic and direct force measurements between silica and mica surfaces in dilute electrolyte solutions, Langmuir **13**, 2207 (1997).